New Journal of Physics
The open–access journal for physics

Modulation of surface plasmon coupling-in by one-dimensional surface corrugation

F López-Tejeira[1], Sergio G Rodrigo[1], L Martín-Moreno[1,9], F J García-Vidal[2], E Devaux[3], J Dintinger[3,7], T W Ebbesen[3], J R Krenn[4], I P Radko[5], S I Bozhevolnyi[5], M U González[6,8], J C Weeber[6] and A Dereux[6]

[1] Departamento de Física de la Materia Condensada, Facultad de Ciencas-ICMA, Universidad de Zaragoza-CSIC, E-50009 Zaragoza, Spain
[2] Departamento de Física Teórica de la Materia Condensada, Universidad Autónoma de Madrid, E-28049 Madrid, Spain
[3] Laboratoire de Nanostructures, ISIS, Université Louis Pasteur, F-67000 Strasbourg, France
[4] Institute of Physics, Karl Franzens University, A-8010 Graz, Austria
[5] Department of Physics and Nanotechnology, Aalborg University, DK-9220 Aalborg, Denmark
[6] Laboratoire de Physique de l'Université de Bourgogne, UMR CNRS 5027, F-21078 Dijon, France
E-mail: lmm@unizar.es

New Journal of Physics **10** (2008) 033035 (19pp)
Received 21 December 2007
Published 27 March 2008
Online at http://www.njp.org/
doi:10.1088/1367-2630/10/3/033035

Abstract. Surface plasmon-polaritons have recently attracted renewed interest in the scientific community for their potential in sub-wavelength optics, light generation and non-destructive sensing. Given that they cannot be directly excited by freely propagating light due to their intrinsic binding to the metal surface, the light–plasmon coupling efficiency becomes of crucial importance for the success of any plasmonic device. Here, we present a comprehensive study on

[7] Present address: Nanophotonics and Metrology Laboratory, Swiss Federal Institute of Technology Lausanne (EPFL), CH-1015 Lausanne, Switzerland.
[8] Present address: ICFO-Institut de Cincies Fotniques, E-08860 Castelldefels, Spain.
[9] Author to whom any correspondence should be addressed.

the modulation (enhancement or suppression) of such a coupling efficiency by means of one-dimensional surface corrugation. Our approach is based on simple wave interference and enables us to make quantitative predictions which have been experimentally confirmed at both the near-infrared and telecom ranges.

Contents

1. Introduction

Surface plasmon-polaritons (SPPs) are electromagnetic (EM) modes originating from the interaction between light and mobile surface charges, typically the conduction electrons in metals [1]. Because of the so-called 'excess of momentum' with respect to light of the same frequency, SPPs cannot propagate away from a planar surface and are thus bound to and guided by it. As a consequence of this binding, SPP modes can be laterally confined below the diffraction limit, which has raised the prospect of SPP-based photonic circuits [2–4]. To build up this kind of circuit, one would require a variety of components in which incident light would be first converted in SPPs, propagating and interacting with different devices before being recovered as freely propagating light. Hence, a great deal of attention has recently been devoted to the creation of optical elements for SPPs [5]–[10], as well as to the efficient coupling of freely-propagating light into and out of them. This latter issue constitutes the fundamental bottleneck that must be overcome in order to fully exploit the potential of SPPs, given that established techniques for SPP generation (which make use of prism [11, 12], grating [13] or nanodefect [14] coupling) require that the system's size be well out of the sub-wavelength scale in order to obtain a neat SPP signal. On the other hand, p-polarized back-side illumination of sub-wavelength apertures in optically thick metal films [15]–[22] prevents both damping and signal blinding but it does not ensure a unique propagation direction for the generated SPPs.

In a previous work [23], we proposed a novel back-side slit-illumination method based on drilling a periodic array of indentations at one side of the slit. It was demonstrated that the SPP beam emerging from the slit to its corrugated side can be backscattered in such a way that it interferes constructively with the one propagating in the opposite direction, thus obtaining a localized unidirectional SPP source. Here, we provide a comprehensive version of our proposal and discuss to some extent its range of validity. Additional experimental measurements will also be presented.

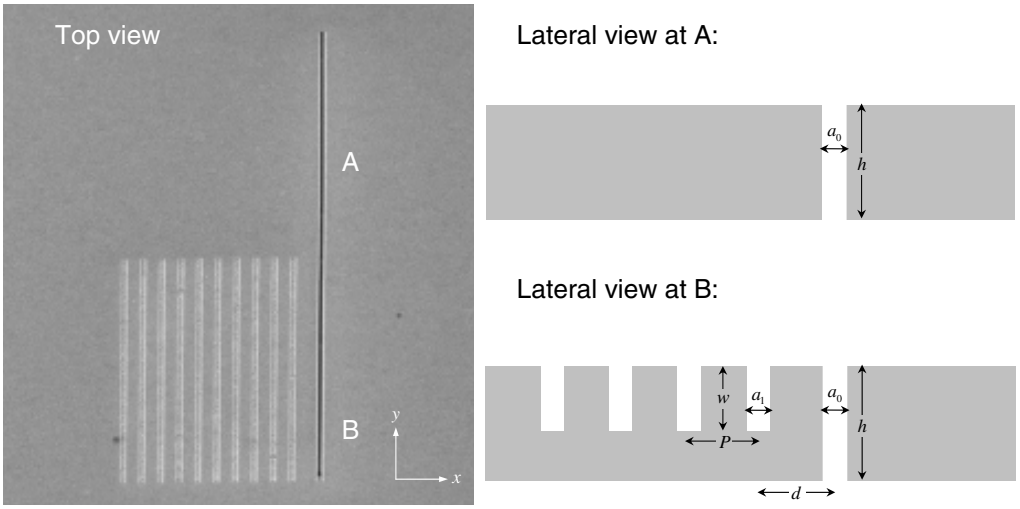

Figure 1. Scanning electron micrograph and schematic diagrams of the proposed structure. Parameters $\{a_i, h, w, d, P\}$ defining the geometry of the system are also shown.

This paper is organized as follows: in section 2, we summarize the key concepts of our proposal and focus on some quantitative aspects of SPP generation and reflection. The validity of our simple wave interference model is discussed in section 3. Finally, experimental results are presented in section 4, prior to the general conclusions.

2. Description of our proposal

A picture of the proposed structure is shown in figure 1. A periodic array of one-dimensional (1D) indentations is fabricated at the output metal surface close and parallel to the illuminated slit. The starting point for such a design can be found in a previous work on 1D SPP scattering by means of a modal expansion formalism [24, 25]. In order to cope with SPP launching, we considered a single slit flanked by an array of indentations (rectangular grooves) placed in the output surface of a thick metallic film. Eventually, the distance between the slit and indentations was taken to be infinity. In this way, the slit merely played the role of a theorist's SPP-launcher, as far as it can be shown that the field created by the slit corresponds to SPP illumination into the grooves. Besides, we also found a simple geometrical condition for the groove array to behave as a perfect Bragg mirror, associated with the low-λ edge of the plasmonic bandgap for the periodic system. Combining these two elements, one can obtain a remarkably simple scheme to modulate the SPP coupling-in at a real back-side illumination experiment: given an incident wavelength, let us design a groove array for which SPP reflectance rises to a maximum and place it at a distance d from the slit (situation B of figure 1). Hence, any outgoing SPP generated at the same side of the slit will be mainly backscattered by the grooves and interfere either constructively or destructively with the one that is generated at the opposite side. This interference can be tuned by adjusting the separation d between the slit and the first groove of the array, defined centre to centre. The total phase difference, ϕ, between the interfering SPPs will then consist of the phase change upon reflection plus the additional shift resulting from the

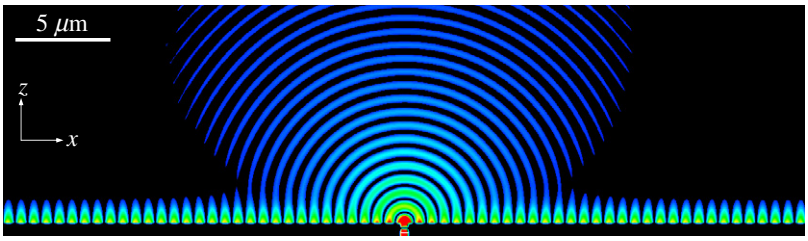

Figure 2. Calculated $|\mathrm{Re}[H_y]|$ distribution at the output surface of an Au film perforated by a single slit (situation A of figure 1). Incident light is p-polarized and impinges normally onto the back side of the metal surface at $\lambda = 800$ nm. Here, slit width $a_0 = 160$ nm and film thickness $h = 300$ nm.

two different path lengths along the metal:

$$\phi = \phi_{\mathrm{R}} + 2\mathrm{Re}[k_{\mathrm{p}}]\, d, \tag{1}$$

where k_{p} holds for in-plane plasmon wavevectors. According to (1), constructive or destructive interference should occur for those phase values equal to, respectively, even or odd multiples of π.

It is clear that, as will be discussed in section 3, several objections may arise against this very simplified model, but before we turn to its validity, let us take a closer look at the two ingredients on which it is based: the generation of SPPs at a sub-wavelength aperture and the phase they acquire as a result of Bragg reflection.

2.1. SPP generation at a single sub-wavelength slit

Figure 2 presents a finite-difference time-domain (FDTD) [26] simulation of the (EM) field distribution originated from p-polarized back-side illumination of a sub-wavelength slit on a thick Au film. As can be seen, the most of the field is diffracted away, but a significant fraction appears to be bound to the metallic surface at each side of the aperture. However, to what extent is that a confined state of surface plasmon?

Such an assessment requires that analytical expressions for the EM field distribution created by the slit be obtained without any *a priori* assumption about the presence of SPPs. For that purpose, we have made use of the above-mentioned modal expansion technique. Given that it has been extensively described elsewhere [24, 25], let us just briefly summarize its basic ingredients: the EM fields are expanded in terms of the eigenmodes in each spatial region (plane waves at input/output regions and waveguide modes inside the indentation) and then the expansion coefficients are obtained by just matching appropriately the parallel components of the fields at the two metal–dielectric interfaces. The dielectric response of the metal is taken into account by applying surface impedance boundary conditions (SIBC) [27] to the tangential components of the EM fields at the metallic surface. For a non-magnetic medium,

$$\boldsymbol{F}_{\mathrm{t}}(\boldsymbol{r}) \equiv \boldsymbol{E}_{\mathrm{t}}(\boldsymbol{r}) - Z_{\mathrm{s}} \boldsymbol{H}_{\mathrm{t}}(\boldsymbol{r}) \times \boldsymbol{n}(\boldsymbol{r}) = 0, \tag{2}$$

where $Z_{\mathrm{s}} = \varepsilon(\lambda)^{-1/2}$ and $\boldsymbol{n}(\boldsymbol{r})$ is the unitary vector normal to the surface directed into the metal half-space. However, SIBC are not applied at the vertical walls defining the slit but for the calculation of propagating constants along the z-direction. This choice allows us to express the EM fields inside in terms of the waveguide eigenmodes of a perfect conductor (PC), which are

known analytically. Although the absorption inside the cavities is therefore neglected, one can expect this not to be a serious shortcoming when considering sizes much greater than the skin depth. The end product of our expanding and matching is a linear system of algebraic equations that connect the modal amplitudes of the $\boldsymbol{F}$ field at the input and output openings of the slit. Once those self-consistent amplitudes are found, it is straightforward to obtain the EM fields at any desired point.

By imposing the constraint that incident light impinges in 'classical mounting' (i.e. within the xz-plane), we just have to concern ourselves with the y-component of the magnetic field. From a mathematical point of view, H_y at the output side is obtained by integrating all across the slit every considered eigenmode ϕ_n multiplied by a scalar 1D Green's function and then weighting each contribution with the corresponding amplitude E'_n at the output opening:

$$H_y(x,z) = -\sum_n E'_n \int_{x_0-a_0/2}^{x_0+a_0/2} \mathrm{d}x' G(x,x';z)\phi_n(x'), \tag{3}$$

where z stands for the distance from the output surface. This closely resembles the Huygens–Fresnel description of wave propagation in terms of a set of point emitters, but we have to keep in mind that all those 'emitters' are self-consistently connected.

However, information on the character of the generated field is contained neither in the modes nor in their amplitudes, but in the propagator itself:

$$G(x,x';z) = \frac{\mathrm{i}}{\lambda}\int_{-\infty}^{+\infty} \mathrm{d}k \frac{\exp[\mathrm{i}(k(x-x') + \sqrt{k_0^2 - k^2}z)]}{\sqrt{k_0^2-k^2}+k_0 Z_\mathrm{s}}, \tag{4}$$

where $k_0 \equiv 2\pi/\lambda$. Despite its impressive appearance, $G(x,x';z)$ just computes the projection of EM fields at the opening of the slit onto all possible diffracted waves, whether they are propagating or evanescent. Bound-to-interface contributions are incorporated into the picture as a consequence of finite Z_s, which makes the difference with respect to PC approximation: for $Z_\mathrm{s} = 0$, (4) transforms into an integral representation of the zeroth-order Hankel function of the first kind (i.e. the well-known Green's function for the two-dimensional Helmholtz operator [28]), otherwise it has to be evaluated numerically. Such a numerical inspection reveals that $G(x,x';z)$ tends to the PC result for $|x-x'| \ll \lambda$ irrespective of Z_s [24, 25]. On the other hand, in the regime where $z, |x-x'| \approx O(\lambda)$, oscillatory contributions within the kernel of (4) mutually cancel everywhere but in the region close to the integrand singularities at $k = \pm k_\mathrm{p}$, with k_p satisfying

$$\sqrt{k_0^2 - {k_\mathrm{p}}^2} = -Z_\mathrm{s} k_0. \tag{5}$$

This is, by the way, the SPP dispersion relation of a flat metal–dielectric interface within the SIBC. In that asymptotic limit, Green's function can be explicitly approximated as

$$G_\mathrm{as}(x,x';z) = -\frac{k_0^2 Z_\mathrm{s}}{k_p}\,\mathrm{e}^{\mathrm{i}(k_\mathrm{p}|x-x'|-k_0 Z_s z)}. \tag{6}$$

Therefore, and even in the presence of absorption, SPPs govern the EM coupling along the surface at a distance of several wavelengths, whereas 'PC-like' behaviour is observed at the close vicinity of the slit. It is worth mentioning that this simple fact is completely misinterpreted in several recent papers, as pointed out in a previous work [29]. In any case, the existence of these two regimes has also been remarked by introducing a 'creeping wave contribution' that

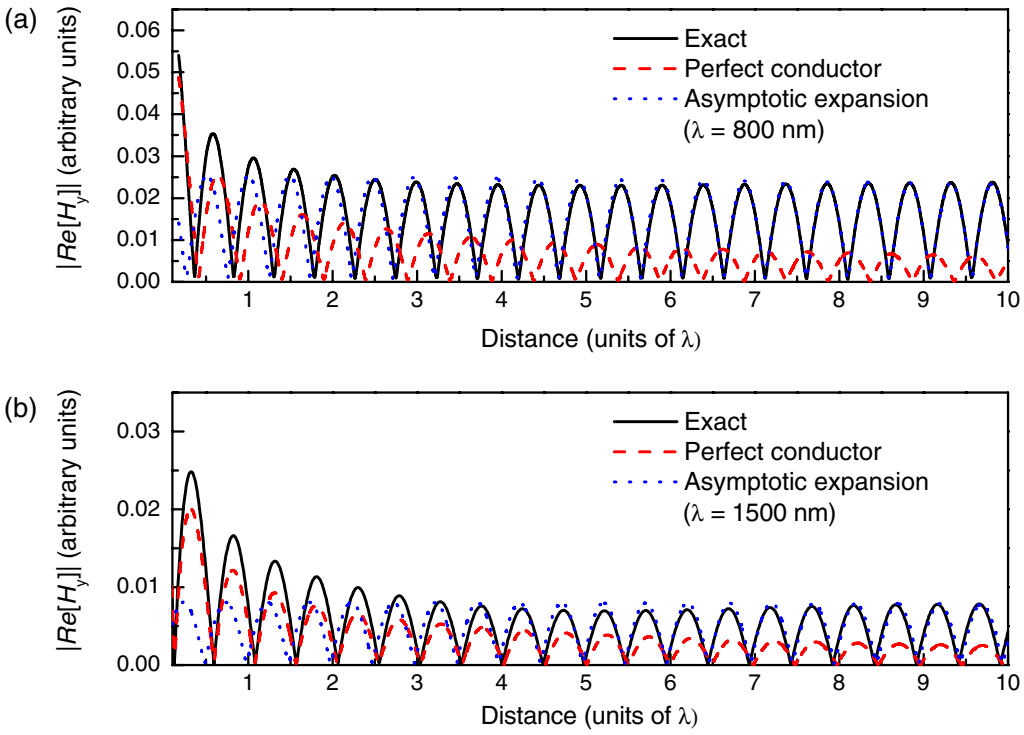

Figure 3. Calculated |Re[H_y]| as a function of the distance from the centre of the slit, evaluated at the output surface of an Au film. Solid lines represent the full calculation, whereas dashed and dotted ones stand for PC approximation and asymptotic expansion, respectively. The geometrical parameters are: slit width $a_0 = 160$ nm and film thickness $h = 300$ nm. Incident light is p-polarized and impinges normally onto the back side of the metal surface. (a) and (b) Results for $\lambda = 800$ and $\lambda = 1500$ nm, respectively.

rapidly vanishes for increasing distances and is explicitly defined as the difference between total and SPP fields along the metal–dielectric interface [30].

In order to determine the precise range of distances for the EM field at figure 2 to be dominated by either 'PC-like' or SPP contribution, we have calculated |Re[H_y]| at the metal surface for Z_s values corresponding to that of Au at 800 and 1500 nm. Each calculation was carried out for the exact, asymptotic and PC versions of Green's function. As can be seen in figure 3, comparison with the exact result in the near-infrared (NIR) shows that the asymptotic limit is already reached for a distance of about 2λ from the centre of the slit, which is increased up to 6λ when the incident wavelength falls within the telecom range. Consequently, it is only for greater distances that we can unambiguously establish a one-to-one correspondence between fields at the interface and SPPs.

In figure 4, we present the fraction of the output current that is transferred into SPPs (f_{SPP}) and scattered out of the plane (f_{out}) for the same Z_s parameters as in figure 3 all across the sub-wavelength regime. Given that SPPs gradually attenuate when propagating along the metal, the values for f_{SPP} are calculated at $x = \pm a_0/2$ in order to compare with those of f_{out}. As the slit width increases, the out-of-plane radiation is clearly favoured at the expense of the coupling

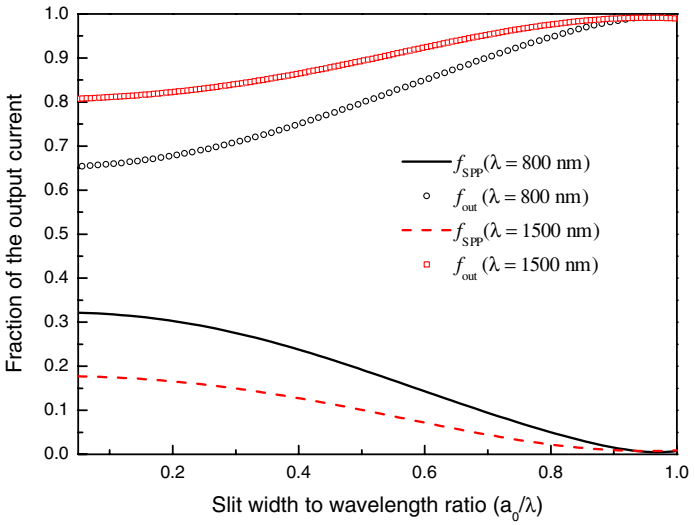

Figure 4. Fraction of the energy that is transferred into SPPs (lines) and scattered out of the plane (symbols) at the output surface of an Au film perforated by a single slit that is back-side illuminated with p-polarized light. The values for f_{SPP} are calculated at distances of $\pm a_0/2$ from the centre of the slit.

into SPPs, which can be easily found to be proportional to $(\sin[k_p\, a_0/2]/k_p\, a_0)^2$ because of the geometry of the system [24, 25]. For typical experimental width $a_0 = 160$ nm, no more than 30% of the output energy is driven into SPPs at $\lambda = 800$ nm and such a percentage is reduced to 17% at $\lambda = 1500$ nm. These values are in good agreement with those previously reported [21] and provide a preliminary estimate of the expected performance for our proposed slit + grating structure when operating at perfect constructive interference conditions.

2.2. Phase shift upon Bragg reflection

As mentioned at the beginning of the section, it has been shown that the reflection of SPPs by a periodic array of indentations presents maxima at those frequencies corresponding to the low-λ edges of plasmonic bandgaps [24, 25]. For narrow sub-wavelength indentations, the spectral locations of these edges can be approximated by folding the dispersion relation of SPPs for a flat metal surface into the first Brillouin zone [31]. Within the SIBC, such a folding results in

$$k_p P = k_0 \mathrm{Re}[q_p] P = m\pi, \quad m = 1, 2, \ldots, \tag{7}$$

where P is the period of array and $q_p \equiv \sqrt{1 - Z_s^2}$. Remarkably, although the reflectance maxima depend on the groove geometry (width and depth) and the number of grooves [24, 25], their spectral locations do not (see figure 5).

Assuming that λ and P fulfil (7), let us consider the phase shift for a given resonant wavelength λ_R. Information on such a shift is contained in the complex reflection coefficient r relating the amplitudes of incident and reflected fields. Although the obtention of r is usually regarded as a mere preliminary to that of reflectance (defined as $R = |r|^2$), we can always establish a straightforward connection between r and phase shift ϕ_R:

$$\cos\phi_R = \mathrm{Re}[r]/|r|; \quad \sin\phi_R = \mathrm{Im}[r]/|r|. \tag{8}$$

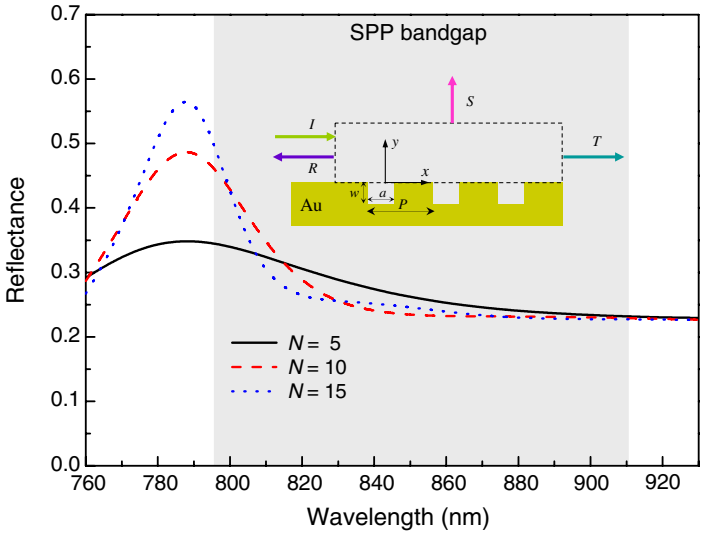

Figure 5. Calculated reflectance of SPPs by a finite periodic array consisting of 5 (solid line), 10 (dashed) and 15 (dotted) grooves carved on Au. Here, $a = w = 100\,\text{nm}$ and $P = 390\,\text{nm}$. Grey-shaded area marks the region where a plasmonic bandgap occurs. SPP fields are evaluated at $x = -3.5\,\mu\text{m}$ ($\approx -3.8\lambda_{\max}$), the origin being located at the centre of the first groove.

Once the asymptotic limit is already reached, these auxiliary magnitudes $\cos\phi_{\text{R}}$, $\sin\phi_{\text{R}}$ provide complete information about SPP shift upon reflection, irrespective of the exact distance at which fields are evaluated. We have found that ϕ_{R} is close to π over a wide range of groove depths for $a/\lambda \leqslant 0.2$ at both NIR and telecom ranges, as can be seen in figure 6. Taking this result into account and substituting for k_{p} from (7) into (1) yields

$$\phi(\lambda_{\text{R}}) = (2md/P + 1)\pi, \tag{9}$$

which reduces the design of our proposed scheme to a suitable choice of the d/P ratio.

3. Validity of the simple wave interference model

Our previous discussion leading to (9) implies that slit and grating be considered as independent elements. Therefore, it does not take into account the radiation coming back from the grooves, while, in principle, EM fields at all openings have to be self-consistently calculated [32]. In order to quantify the 'perturbation' of the SPP source (i.e. the slit), we define a re-illumination parameter ξ that averages the modification of the x-component of the electric field inside the slit originated by the adjacent grating:

$$\xi = \frac{1}{a_0}\int_{-a_0/2}^{+a_0/2} \mathrm{d}x' |1 - E_x(x')/E_x^{ss}(x')|, \tag{10}$$

where a_0 is the width of the slit, E_x the x-component of the electric field calculated in the presence of the array and E_x^{ss} the one obtained for the isolated slit.

In figure 7, we present a contour plot of ξ versus groove depth and slit-to-array separation for a system with ten grooves at $\lambda = 800\,\text{nm}$. As can be seen, the modification of the field

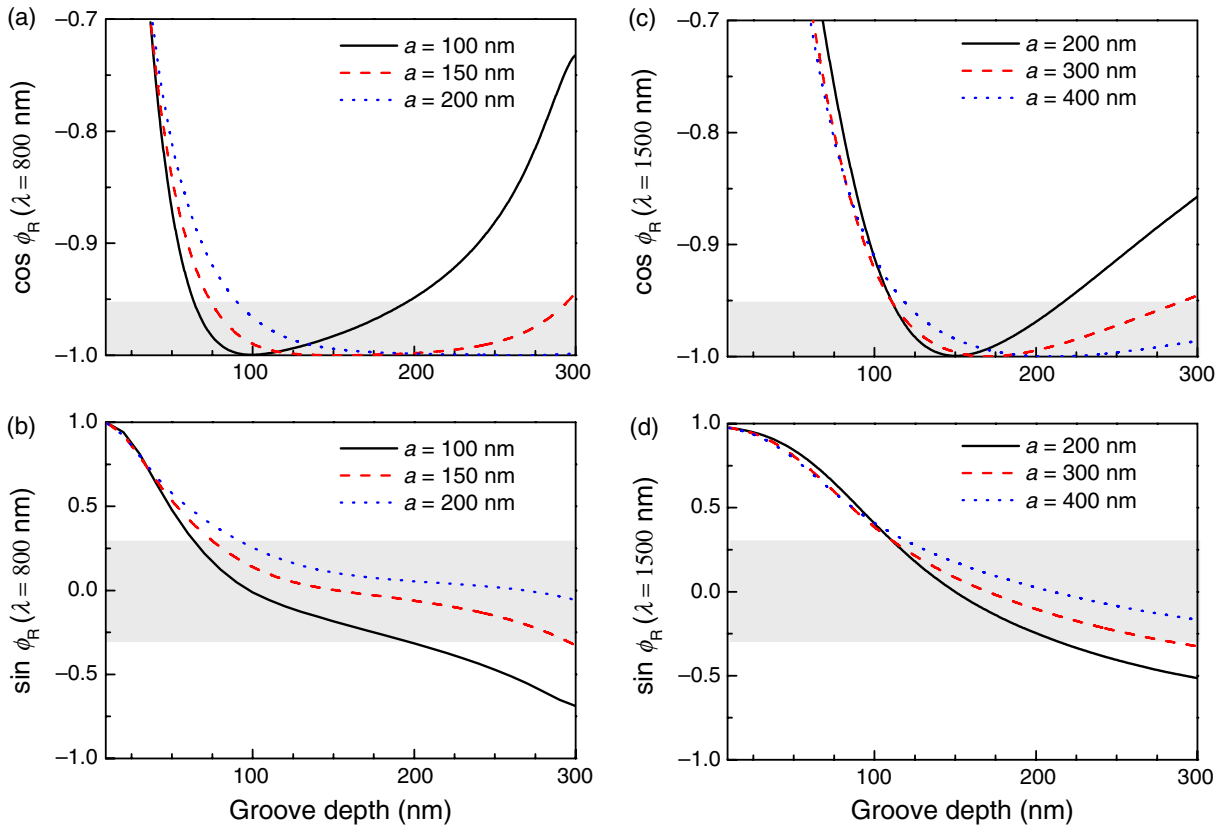

Figure 6. Calculated values of $\cos\phi_R(\lambda_R)$, $\sin\phi_R(\lambda_R)$ of a ten-groove array in Au for increasing values of groove depth. (a) and (b) Results for $a = 100$, 150 and 200 nm (solid, dashed and dotted lines, respectively) evaluated at $\lambda_R = 800$ nm ($P = 390$ nm, $m = 1$). Results for $a = 200$, 300 and 400 nm at $\lambda_R = 1500$ nm ($P = 750$ nm, $m = 1$) are presented in (c) and (d). Grey-shaded areas mark the region where $\phi_R = \pi \pm 0.1\pi$. Results for $\lambda_R = 800$ and 1500 nm are calculated at distances of 3λ and 7λ from the centre of the first groove, respectively.

pattern within [400, 800] nm is below 15% and ξ rapidly decreases for increasing distances, thus supporting our implicit assumption in (9). With respect to the dependence on groove depth, it is governed by the reflectance properties of the array, ξ rising to its maximum as R does (see the inset in figure 7). Such a maximum becomes clearer the more separation approaches to the plasmonic regime ($d \approx 3\lambda$). On the other hand, modulation along the vertical axis results from simple interference between counter-propagating SPP waves originated at the slit and its nearest groove. Therefore, sequential minima of ξ appear for $d = (2m+1)\lambda_p/4$, whereas $\{\xi_{max}\}$ are associated with $d = m\lambda_p/2$, given that $\lambda_p = 2\pi/k_p$ and $m = 0, 1, 2, \ldots$.

However, the key point of our proposal still relies on SPPs being reflected by a groove array, while the EM fields radiated by the slit cannot be considered 'purely plasmonic' but at a distance of several wavelengths (see figure 3). In order to characterize the efficiency of the slit + array system as an SPP-launcher for any slit-to-array separation, we introduce its 'efficiency ratio', E_R: given that the array be located at the left side of the slit (see figure 3), E_R is defined as the quotient between the current intensity of right-propagating SPP with and without

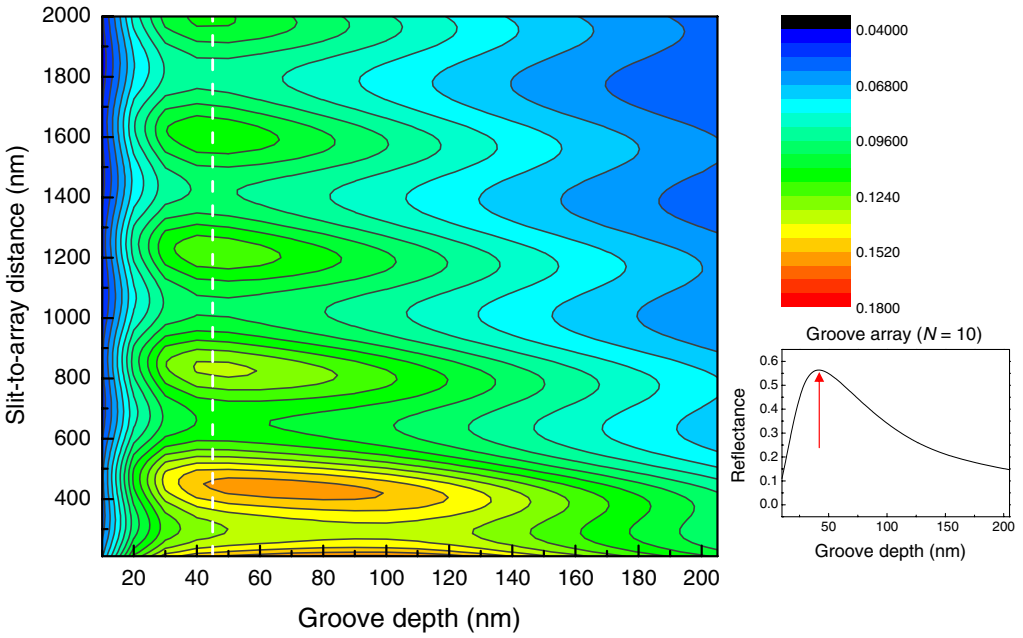

Figure 7. Contour plot of re-illumination parameter ξ in Au as a function of groove depth and slit-to-array separation. Here $a_0 = a_1 = 160\,\text{nm}$, $P = 390\,\text{nm}$, $N = 10$ and $\lambda = 800\,\text{nm}$. The vertical dashed line marks the maximum value of the reflectance curve for the isolated groove array, which is presented at the lower right inset panel.

the grooves. Strictly speaking, E_R provides the efficiency of the output side of the device. The total efficiency, defined as the percentage of incident energy transferred onto the plasmon channel, strongly depends on the illuminating set-up. E_R should vary within the interval $[0, 4]$ showing a dependence on the distance between the illuminating slit and the groove array. More importantly, $E_\text{R} > 2$ implies that the right-propagating SPP current in the presence of grooves is larger than the total SPP current (left+right-moving) in the single slit case, so some of the power radiated out of the plane is redirected onto the SPP channel. According to our simple wave interference model,

$$E_\text{R} \approx |1 + r\, \text{e}^{2\text{i}k_\text{p}d}|^2, \tag{11}$$

where r is the complex reflection coefficient of the groove array for SPPs.

To check the validity of (9) and (11) for slit-to-array separations outside the asymptotic regime, we have carried out numerical calculations of EM fields by means of both modal expansion and FDTD. The system under consideration is intended to operate at a wavelength of 800 nm on a gold film [33]. We consider an array of ten grooves with a period $P = 390\,\text{nm}$. The depth of the grooves is chosen to be $w = 100\,\text{nm}$, while the width of both grooves and slit is $a = 160\,\text{nm}$, which are typical experimental parameters. Figure 8(a) shows the comparison between (11) and numerical evaluations of E_R, as well as the location of interference maxima (vertical lines) predicted by (9) for $m = 1$. The agreement between the modal expansion and FDTD results is excellent but for distances at which intra-wall coupling between the slit and the first groove has to be taken into account ($d \approx 2a$). As can be seen, the locations of maximum E_R are accurately predicted by (9), which allows us to design SPP-launchers without

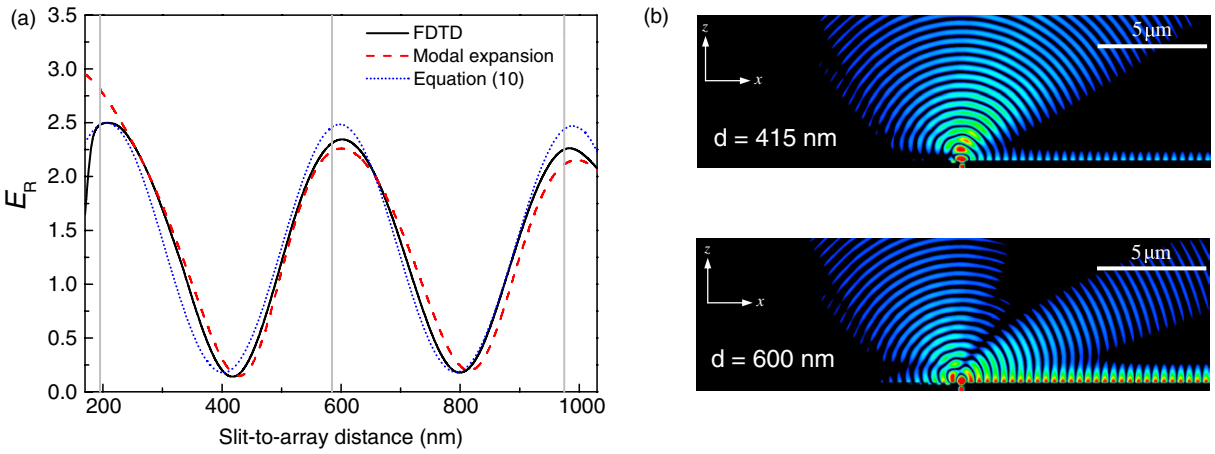

Figure 8. Numerical results for the SPP-launcher at wavelength $\lambda = 800$ nm. (a) Dependence of the efficiency ratio E_R on the slit-to-array distance. The geometrical parameters defining the system are: slit and groove widths $a = 160$ nm, groove depth $w = 100$ nm and array period $P = 390$ nm. The figure renders the curves obtained by means of FDTD (solid), modal expansion (dashed) and equation (11) (short-dotted). Vertical lines mark the positions of E_R maxima according to (9). (b) Calculated $|\mathrm{Re}[H_y]|$ distributions over the xz-plane for two different distances corresponding to minimum and maximum values of E_R at $\lambda = 800$ nm.

elaborate numerical calculations. Moreover, the simplified model of (11) provides a good approximation to E_R with the sole input of r. This also implies that non-plasmonic contributions to groove illumination play a minor role in the occurrence of either constructive or destructive interference, which is clearly described by (11) with the exception of minor shifts.

In addition to the efficiency ratio, field patterns in both minimum and maximum conditions were also calculated using the FDTD method. As shown in figure 8(b), SPPs are completely absent from the left side of the slit, whereas field intensity at the right side of the slit is clearly modulated by the slit-to-array separation, which also governs the spatial distribution of the field that is radiated into vacuum.

4. Experimental results

4.1. NIR measurements

For our proposal to be tested out at the NIR regime, several slit + array samples were fabricated on gold films with a focused ion beam (FIB). As described in [23], each sample consists of a single long ($L = 30\,\mu$m) slit of width $a_0 = 160$ nm perforated at a 300-nm-thick film that is flanked by a periodic array of grooves ($P = 390$ nm, $a = 160$ nm, $w = 100$ nm). Such an array is placed at a given distance d and only extends over $L/2$ (see figure 1). This kind of sample enables us to measure E_R, as the upper part can be used as an on-chip reference of the 'isolated slit'.

A set of samples with $d = \{195, 292, 390, 486, 585\}$ nm was imaged at 800 nm by a photon scanning tunnelling microscope (PSTM) making use of an incident focused beam illumination.

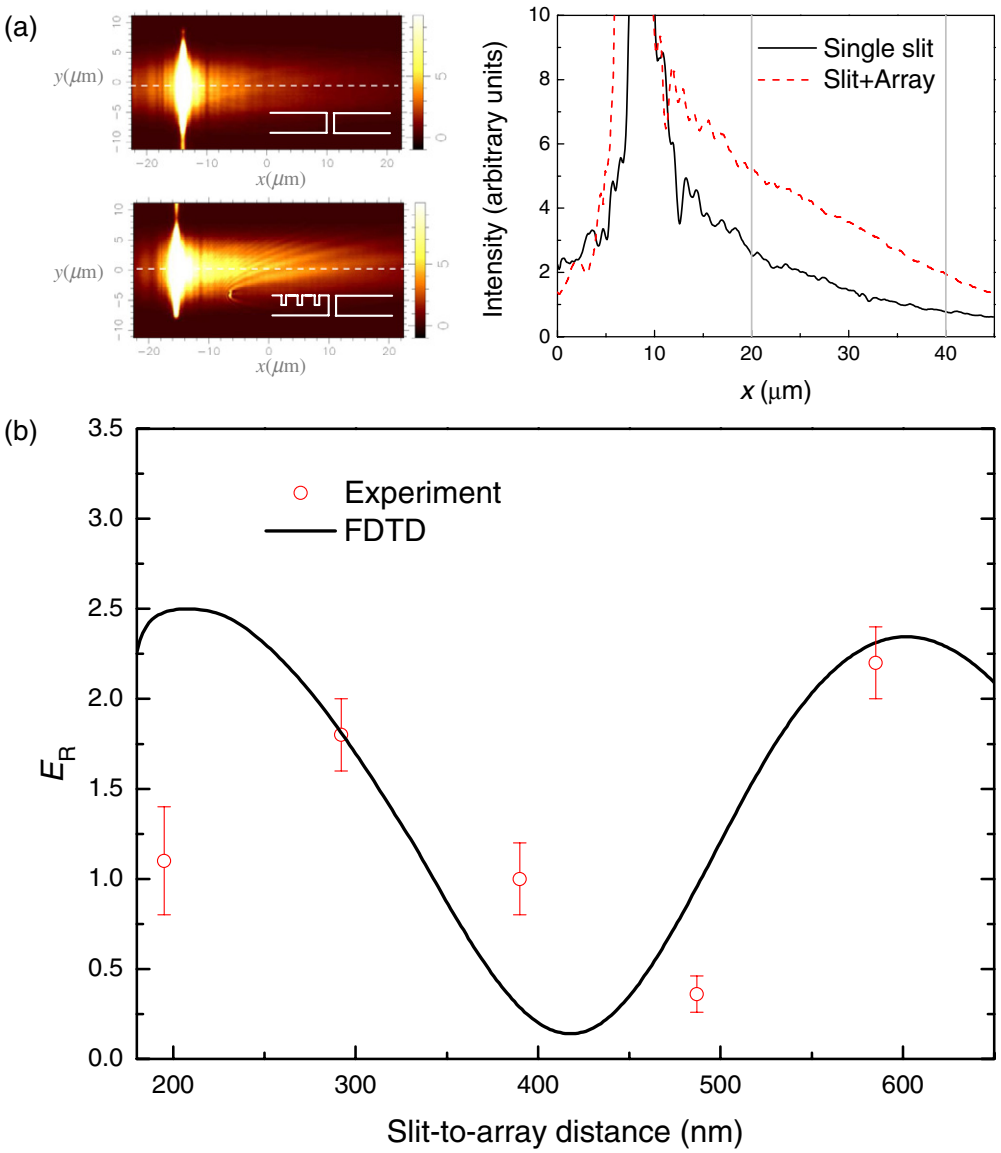

Figure 9. Experimental measurement of E_R at $\lambda = 800$ nm for the same geometrical parameters as in figure 8. (a) PSTM micrographs recorded for a sample with $d = 585$ nm at both 'single slit' (top) and slit + array configurations (bottom). The right panel shows the two cross-cuts from which E_R is obtained. Vertical lines define the interval along which the ratio is averaged. (b) Experimental (circles) and numerical (solid line) values of E_R as a function of slit-to-array distance. The error bars represent the standard deviation over a set of different structures with the same nominal parameters.

For each sample, a pair of images was recorded by scanning at a constant distance of about 60–80 nm from the surface (see figure 9(a)). The first image of the pair, corresponding to an SPP generated from a single slit, is obtained by focusing the laser beam on the upper part of the slit. For the second image, the laser beam is moved to the lower part in order to collect the data for the slit + array structure. An average longitudinal cross-cut of each image is obtained by

using 20 longitudinal cross-cuts, corresponding to different coordinates along the slit axis. Then, the relative position of the two average cross-cuts is adjusted so that the saturated areas (i.e. the signal taken right on top of the slit) are superimposed. Finally, the experimental efficiency ratio, E_R, is extracted by averaging the ratio between the two curves along the longitudinal cross-cut. Figure 9(b) renders experimental values (circles) of E_R for the five different samples fabricated, as well as the ones obtained from FDTD simulations (solid line). The concordance between measurements and theoretical predictions is quite remarkable, especially when taking into account that each experimental point corresponds to an average over a different set of samples. We find that this agreement (previously reported in [23]) provides a clear support to our proposal for a localized unidirectional SPP source.

Another way of looking at the role of surface corrugation is to consider its influence on the fraction of the output energy that is radiated into vacuum. Given that some of the radiated power is redirected onto the SPP channel for the condition of maximum E_R (see field pattern at figure 8), we may wonder whether or not the radiated field is also modulated by the slit-to-array separation. For that purpose, a new magnitude E_{out} can be defined as the ratio between the radiated energy with and without the grooves. According to our numerical simulations, such an 'out-of-plane efficiency' presents a similar (but opposite) dependence on d to that of E_R. In order to obtain experimental values for E_{out}, a new type of sample was designed (see figure 10(a)). Now, the illuminating slit is flanked by two-groove arrays with the same periodicity $P = 390$ nm, each one extending over $L/3$. No corrugation is present at the middle part of the system, for it to be used as the 'single slit' reference. The array on the top is located at a distance $d_1 = 607$ nm for which the coupling to SPPs rises to a maximum at $\lambda = 800$ nm, whereas a minimum appears for the distance $d_2 = 404$ nm of the bottom one. Consequently, the far-field radiation pattern of the composed structure is expected to present a $d_1 \rightarrow d_2$ ascending staircase profile.

In figures 10(b) and (c), we present PSTM images recorded at 800 and 3000 nm from the surface of the sample. As can be seen, the intensity distribution along the illuminating slit increases from the upper to the middle third, as well as from the middle to the lower. Although this behavior is in qualitative agreement with our predictions, a rigorous determination of E_{out} would have required extensive measurements similar to those of E_R. Unfortunately, such a procedure became impossible because of accidental fatal damage in the sample. However, we have managed to obtain a rough estimate of E_{out} from available PSTM images: dashed rectangles in figures 10(b) and (c) mark the areas over a four-line average ($\approx$625 nm) longitudinal cross-cut of each image obtained by means of WSxM software [34]. The resulting intensity profiles at figure 10(d) and (e), show a clear succession of steps, which we decide to characterize by the arithmetic mean along the 5-micron central segment of each plateau. Numerical estimates of E_{out} are then calculated as the ratio between d_1, d_2 and single slit values (see table at the bottom left of figure 10). The coincidence of those estimates with the calculated E_{out} curve in figure 10(f) is amazingly good, which encourages us to carry out conclusive measurements in the near future. With respect to figure 10(f), we finally have to remark that the radiative-to-SPP conversion seems to be more efficient than its opposite, as far as $E_{out} < 2$ for any d.

4.2. Telecom measurements

Similar samples to those used in the NIR measurements were designed to operate at the telecom range by upscaling the period of the array and its separation from the slit (see figure 11(a)).

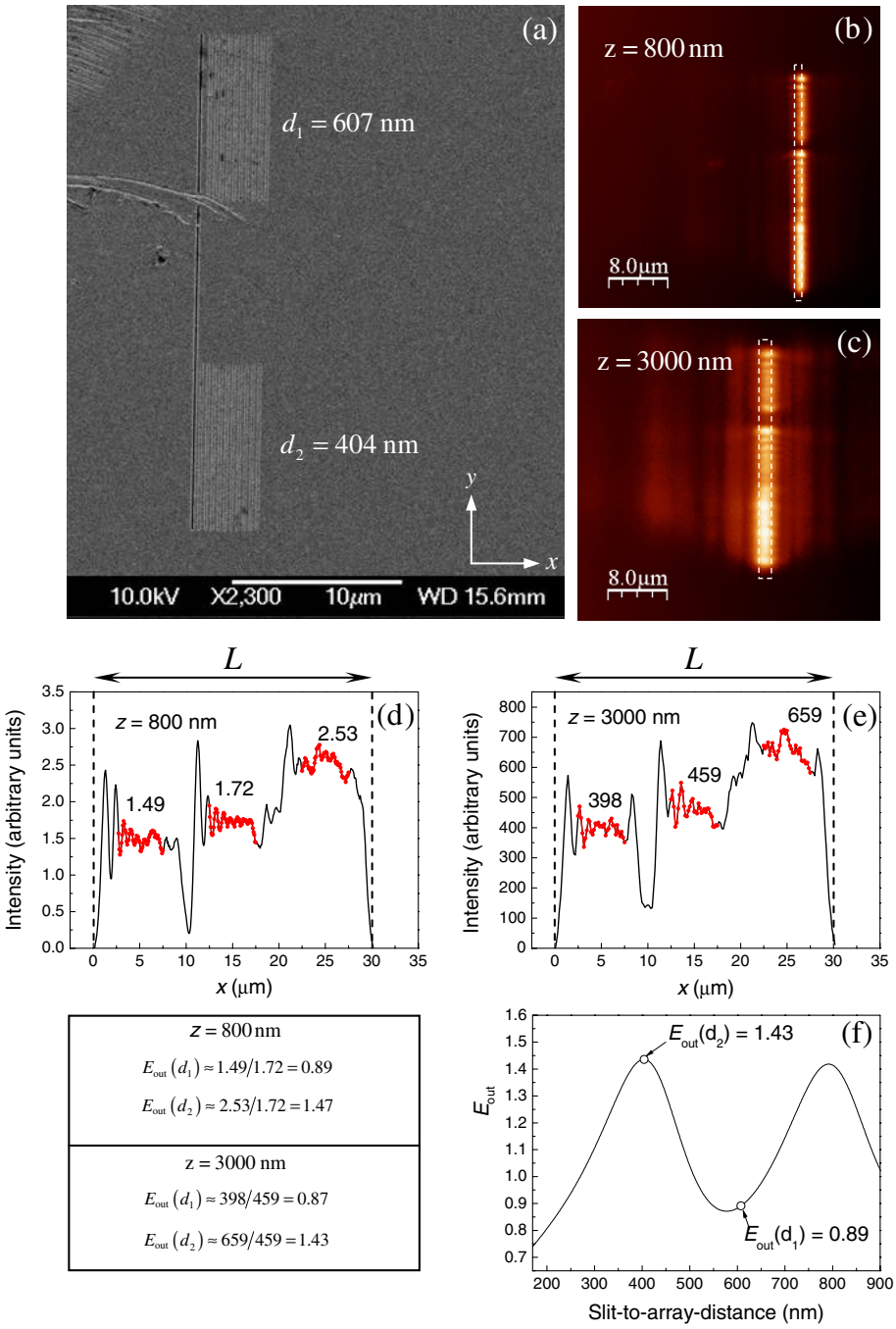

Figure 10. Experimental estimate of E_{out} at $\lambda = 800$ nm. (a) Scanning electron micrograph of the sample. The geometrical parameters are: slit length $L = 30\,\mu$m, slit width $a_0 = 104$ nm, groove width $a = 75$ nm, groove depth $w = 100$ nm and array period $P = 390$ nm. (b) and (c) PSTM micrograph recorded at distances of 800 and 3000 nm from the metal surface. (d) and (e) Average longitudinal cross-cuts along dashed rectangles in images (b) and (c). Vertical dashed lines mark the position of the slit. (f) Calculated E_{out} as a function of slit-to-array distance. Lower left table: summary of the experimental estimates of E_{out}.

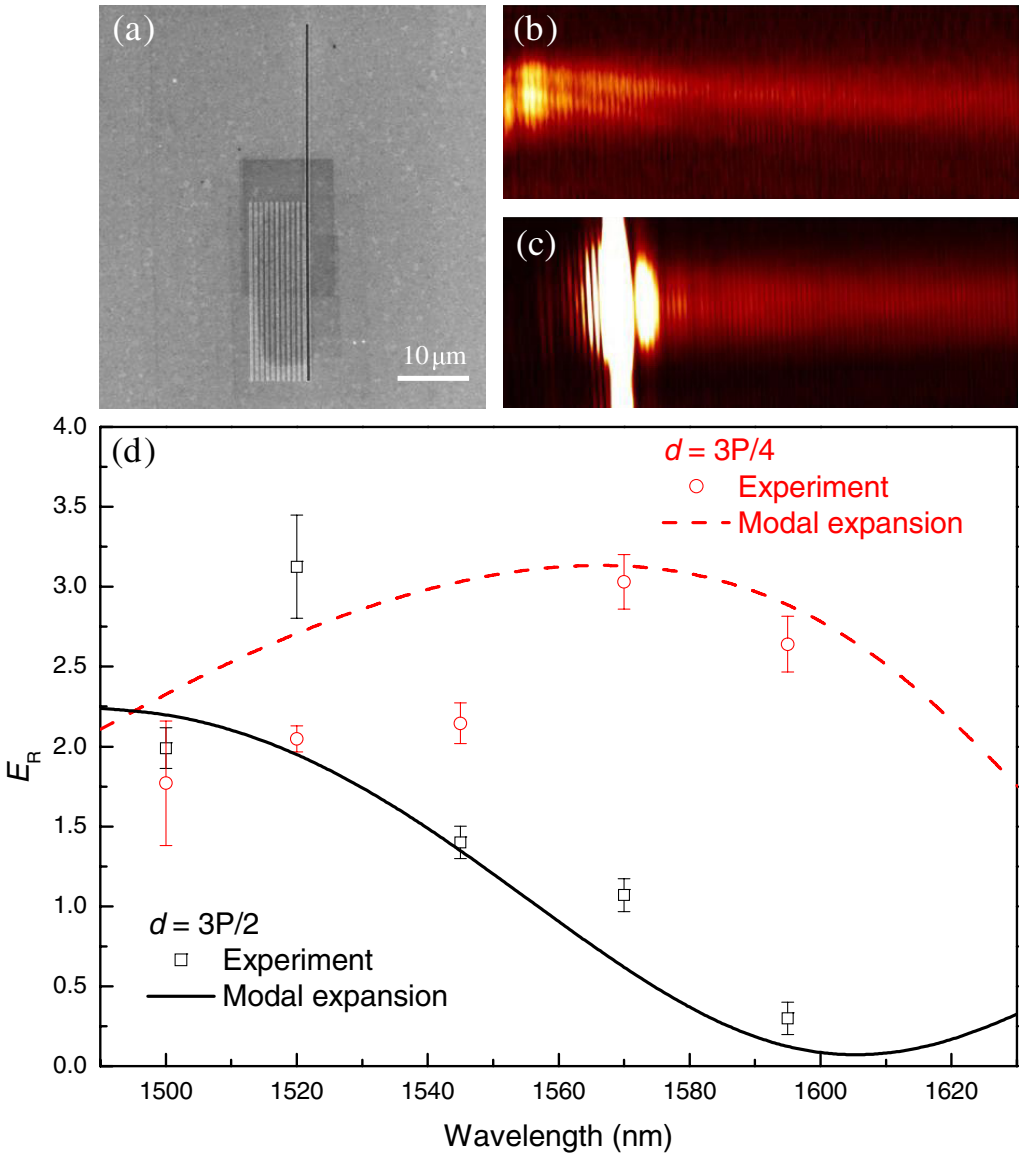

Figure 11. Spectral dependence of E_R at the telecom range. (a) Scanning electron micrograph of the sample. The geometrical parameters are: slit length $L = 50\,\mu$m, slit width $a_0 = 400$ nm, groove width $a = 200$ nm, groove depth $w = 100$ nm and array period $P = 750$ nm. (b) Near-field image recorded with the laser beam focused at the 'isolated slit' position of a sample with $d = 3P/2 = 562$ nm. (Size $= 70 \times 26\,\mu\text{m}^2$, $\lambda = 1520$ nm.) (c) Same for slit + array focusing. (d) Spectral dependence of E_R for slit-to-array distances of $d = 3P/2 = 1125$ nm (experiment: squares; theory: solid line) and $d = 3P/4 = 562$ nm (experiment: circles; theory: dashed line).

However, in this wavelength regime, we found a kind of instability in the illumination setup that resulted in a noticeable variation of SPP intensity during the near-field scan process, which takes about 45 min per image. As a consequence of those intensity jumps, the technique used to evaluate the 'efficiency ratio' in the NIR became unsuitable. Instead, we found E_R as the SPP

signal ratio taken from each pair of near-field images (with and without side grooves) at the same distance from the slit, where its non-plasmonic field contribution can be disregarded, whereas the SPP signal is still substantial for the quantification ($\approx$50 μm). To decrease the uncertainty of the thus obtained efficiency, a series of scans were performed for every structure and wavelength measurements, conducting independent adjustments, with the subsequent averaging of the E_R values obtained. Hence, the error of E_R represents a statistically estimated deviation.

A typical pair of near-field optical images is presented in figures 11(b) and (c). For telecom wavelengths, the SPP propagation length is increased up to $\approx$200 μm. Figure 11(c) features a strong SPP beam propagating away from the slit in the direction opposite to the array and thereby demonstrating unidirectional SPP excitation. Averaged results and estimated errors for E_R (previously reported in [23]) are rendered in figure 11(d). Notice that the validity of our proposal is now tested in a different way: for a given slit-to-array separation, E_R is measured within the wavelength range 1500–1620 nm, so that the phase difference described by (1) is changed with the increasing wavelength, providing the conditions for constructive or destructive interference. Obviously, this spectral dependence of the efficiency is different for different slit-to-array separations, and we support that experimentally. For the case of the sample with $d = P + P/2 = 1125$ nm, E_R decreases as the wavelength increases (with the only exception of a sharp peak at 1520 nm), evolving from a favorable regime ($E_R \approx 2$) to one in which coupling into SPPs is clearly diminished by the array ($E_R < 1$). Conversely, $E_R \approx 2$ for the sample with $d = 3P/4 = 562$ nm all over the range. As can be seen, the comparison between experiments and modal expansion calculation is rather satisfactory.

Finally, we have to mention that the proposed approach for the excitation of localized unidirectional SPP beams can also be combined with the appropriate design modifications to create functional components for SPP focusing to a spot or tuning the SPP beam divergence. If $E_R \geqslant 2$ is expected for a given slit + array set, its circular bending may produce a converging Gaussian beam whose waist length and radius can be adjusted by means of the curvature. Several curved SPP focusers have been previously achieved [35]–[39], but we find the mirror-blocked back-propagation to be a plus. Although the rigorous modelling of SPP coupling at curved structures is rather complicated and falls out of the scope of the present work, we expect (9) to still provide a good estimation for the proper design of the structure, at least as a starting point. On that assumption, we have fabricated several samples consisting of an arc-of-a-circle slit flanked by the corresponding array of parallel bent grooves (see figures 12(a)–(c)). Geometrical parameters a_0, a, w and P are the same as in figure 11, whereas slit-to-array distance is set to $d = 3P/2 = 1125$ nm.

As shown in figures 12(d)–(f), the effect of SPP launching and focusing can be appreciated already at the stage of far-field adjustment due to weak out-of-plane SPP scattering by surface roughness. Near-field images of SPP excitation on those structures recorded at free-space wavelength of 1520 nm are presented in figure 13. These images clearly demonstrate the property of a curved slit to excite a convergent SPP beam, with the effect being sufficiently enhanced due to the side grooves (cf [36, 37]). With the smallest radius of curvature (30 μm), focusing to a confined spot having size $3 \times 3\,\mu\text{m}^2$ is observed (see the cross-cuts in the lower left panel of figure 13). The SPP beams excited on the less curved structures feature an extended waist (figures 13(b) and (c)), which scales (at least visually) according to expectations, providing a wider, and hence less divergent, SPP beam. That might be useful for particular applications, e.g. in sensing of elongated biological samples or in coupling to low-numerical-aperture waveguides.

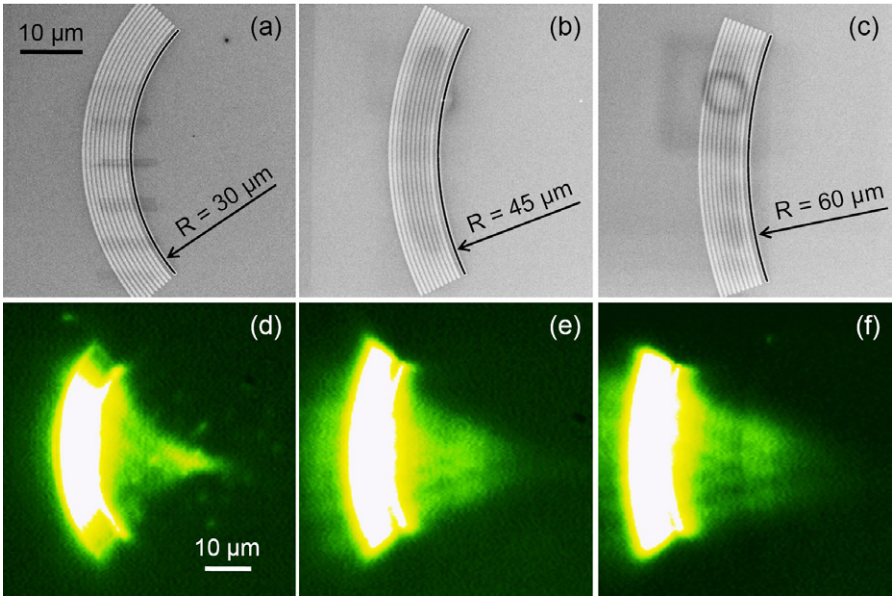

Figure 12. (a) Scanning electron micrograph of the curved structure, characterized by slit and groove widths of 400 and 200 nm, respectively, groove periodicity $P = 750$ nm, groove depth $w = 100$ nm and slit–groove distance $d = 1125$ nm. Film thickness $h = 280$ nm, curvature radius $R = 30\,\mu$m and slit chord length $L = 40\,\mu$m. (b) and (c) Same for $R = 45\,\mu$m and R = 60 μm. (d)–(f) Far-field images of SPPs excited on the structures (a), (b) and (c), respectively, recorded with a charge-coupled device camera.

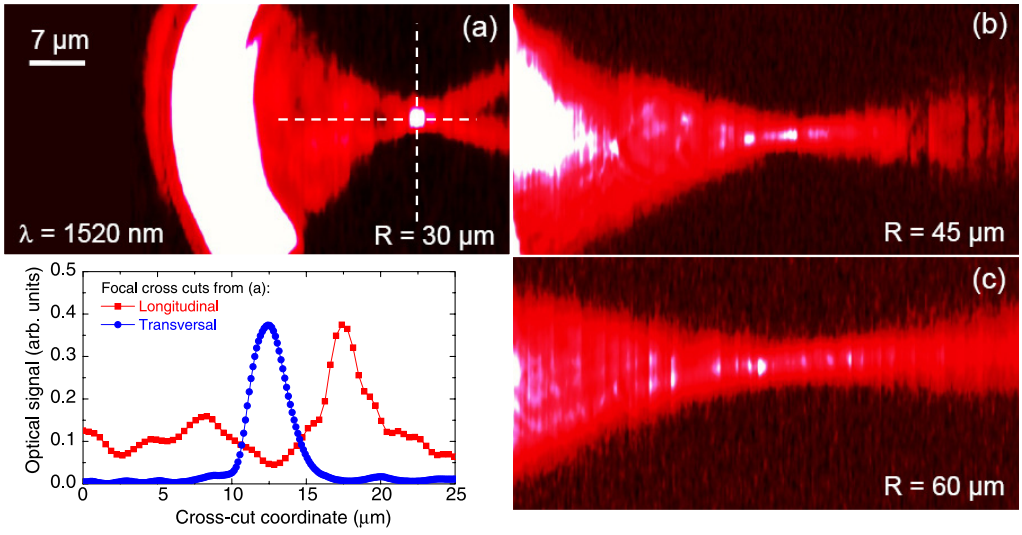

Figure 13. (a)–(c) Near-field images (size $64 \times 32\,\mu$m^2) of SPPs excited on the structures in figure 12 at $\lambda = 1520$ nm. Lower left panel depicts cross cuts obtained from (a) by dissecting the SPP focal spot along longitudinal and transversal directions.

5. Conclusions

In conclusion, we have studied the SPP coupling-in at sub-wavelength apertures with back-side illumination, presenting a novel proposal for the modulation of such a coupling-in by means of a finite array of grooves. Our approach is based on a simple wave interference model that, irrespective of the simplified description of some of the physics involved, has been found to be in good agreement with both sophisticated computer simulations and experimental measurements at NIR and telecom ranges. We find this to constitute a stimulating challenge for further developments on a wide range of SPP devices.

Acknowledgments

Financial support by the EU (project FP6-2002-IST-1-507879) and Spanish MEC (project MAT2005-06608-C02-02) is gratefully acknowledged. We thank J-Y Laluet for technical assistance.

References

[1] Raether H 1988 *Surface Plasmons* (Berlin: Springer)
[2] Barnes W L, Dereux A and Ebbesen T W 2003 *Nature* **424** 824
[3] Maier S A 2005 *Curr. Nanosci.* **1** 17
[4] Ozbay E 2006 *Science* **311** 189
[5] Weeber J C, Krenn J R, Dereux A, Lamprecht B, Lacroute Y and Goudonnet J P 2001 *Phys. Rev.* B **64** 045411
[6] Krenn J R, Ditlbacher H, Schider G, Hohenau A, Leitner A and Aussenegg F R 2003 *J. Microsc.* **209** 167
[7] Weeber J C, Lacroute Y, Dereux A, Devaux E, Ebbesen T W, González M U and Baudrion A L 2004 *Phys. Rev.* B **70** 235406
[8] Gómez-Rivas J, Kuttge M, Kurz H, Haring-Bolivar P and Sánchez-Gil J 2006 *Appl. Phys. Lett.* **88** 082106
[9] Bozhevolnyi S I, Volkov V S, Devaux E, Laluet J Y and Ebbesen T W 2006 *Nature* **440** 508
[10] González M U, Weeber J C, Baudrion A L, Dereux A, Stepanov A L, Krenn J R, Devaux E and Ebbesen T W 2006 *Phys. Rev.* B **73** 155416
[11] Otto A 1968 *Z. Phys.* **216** 398
[12] Lamprecht B, Krenn J R, Schider G, Ditlbacher H, Salerno M, Felidj N, Leitner A, Aussenegg F R and Weeber J C 2001 *Appl. Phys. Lett.* **79** 51
[13] Ritchie R H, Arakawa E T, Cowan J J and Hamm R N 1968 *Phys. Rev. Lett.* **21** 1530
[14] Ditlbacher H, Krenn J R, Felidj N, Lamprecht B, Schider G, Salerno M, Leitner A and Aussenegg F R 2002 *Appl. Phys. Lett.* **80** 404
[15] Sönnichsen C, Duch A C, Steininger G, Koch M, von Plessen G and Feldmann J 2000 *Appl. Phys. Lett.* **76** 140
[16] Devaux E, Ebbesen T W, Weeber J C and Dereux A 2003 *Appl. Phys. Lett.* **83** 4936
[17] Yin L, Vlasko-Vlasov V K, Rydh A, Pearson J, Welp U, Chang S H, Gray S K, Schatz G C, Brown D E and Kimball C W 2004 *Appl. Phys. Lett.* **85** 467
[18] Popov E, Bonod N, Nevière M, Rigneault H and Lenne P F 2005 *Appl. Opt.* **44** 2332
[19] Agrawal A, Cao H and Nahata A 2005 *New J. Phys.* **7** 249
[20] Chang S H, Gray S K and Schatz G C 2005 *Opt. Express* **13** 3150
[21] Lalanne P, Hugonin J P and Rodier C 2005 *Phys. Rev. Lett.* **95** 263902
[22] Aigouy L, Lalanne P, Hugonin J P, Julié G, Mathet V and Mortier M 2007 *Phys. Rev. Lett.* **98** 153902
[23] López-Tejeira F *et al* 2007 *Nat. Phys.* **3** 324
[24] López-Tejeira F, García-Vidal F J and Martín-Moreno L 2005 *Phys. Rev.* B **72** 161405

[25] López-Tejeira F, García-Vidal F J and Martín-Moreno L 2007 *Appl. Phys.* A **89** 251
[26] Taflove A and Hagness S C 2000 *Computational Electrodynamics: The Finite-Difference Time-Domain Method* (Boston: Artech House)
[27] Jackson J D 1975 *Classical Electrodynamics* 2nd edn (New York: Wiley)
[28] Arfken G 1985 *Mathematical Methods for Physicists* 3rd edn (San Diego: Academic)
[29] García-Vidal F, Rodrigo S G and Martín-Moreno L 2006 *Nat. Phys.* **2** 790
[30] Lalanne P and Hugonin J 2006 *Nat. Phys.* **2** 551
[31] Kitson S C, Barnes W L and Sambles J R 1996 *Phys. Rev. Lett.* **77** 2670
[32] Martín-Moreno L, García-Vidal F J, Lezec H J, Degiron A and Ebbesen T W 2003 *Phys. Rev. Lett.* **90** 167401
[33] Vial A, Grimault A, Macias D, Barchesi D and de la Chapelle M 2005 *Phys. Rev.* B **71** 085416
[34] Horcas I, Fernández R, Gómez-Rodríguez J, Colchero J, Gómez-Herrero J and Baró A M 2007 *Rev. Sci. Instrum.* **78** 013705
[35] Nomura W, Ohtsu M and Yatsui T 2005 *Appl. Phys. Lett.* **86** 181108
[36] Yin L, Vlasko-Vlasov V K, Pearson J, Hiller J M, Hua J, Welp U, Brown D E and Kimball C W 2005 *Nano Lett.* **5** 1399
[37] Liu Z, Steele J M, Srituravanich W, Pikus Y, Sun C and Zhang X 2005 *Nano Lett.* **5** 1726
[38] Offerhous H L, van der Bergen B, Escalante M, Segerink F B, Korterik J P and van Hulst N F 2005 *Nano Lett.* **5** 2144
[39] Steele J M, Liu Z, Wang Y and Zhang X 2006 *Opt. Express* **14** 5664